JOURNAL OF GEOPHYSICAL RESEARCH, VOL. 106, NO. C7, PAGES 13,989–14,000, JULY 15, 2001

Remapping the thickness distribution in sea ice models

William H. Lipscomb

Los Alamos National Laboratory, Los Alamos, New Mexico

Abstract. In sea ice models with multiple thickness categories the ice thickness distribution evolves in time. The evolution of the thickness distribution as ice grows and melts is analogous to one-dimensional fluid transport and can be treated by similar numerical methods. One such method, remapping, is applied here. Thickness categories are represented as Lagrangian grid cells whose boundaries are projected forward in time. The thickness distribution is approximated as a linear or quadratic polynomial in each displaced category, and ice area and volume are transferred between categories so as to restore the original boundaries. In simple test problems and in a single-column model with forcing typical of the central Arctic, remapping performs significantly better than methods previously used in sea ice models. It is less diffusive than a scheme that fixes the ice thickness in each category and behaves better numerically than a scheme that represents the thickness distribution as a set of delta functions. Also, remapping converges faster (i.e., with fewer thickness categories) than the alternative schemes. With five to seven categories the errors due to finite resolution of the thickness distribution are much smaller than the errors due to other sources. Linear remapping performs as well as the more complex quadratic version and is recommended for climate modeling. Its computational cost is minimal compared to other sea ice model components.

1. Introduction

Most climate models to date have assumed that sea ice has a single uniform thickness in each grid cell. This assumption simplifies the models but is physically unrealistic. In the central Arctic, for example, the mean ice thickness is 2–4 m, but much of the ocean is covered by thin first-year ice and thick pressure ridges. The mean ice thickness, ice strength, surface energy fluxes, and other quantities important for climate depend crucially on the ice thickness distribution [e.g., *Maykut*, 1982; *Schramm et al*., 1997; *Bitz et al*., 2001]. Models with a single ice category, plus open water, can be tuned to give reasonable thicknesses, velocities, and fluxes in the present climate but are likely to have the wrong sensitivities to climate change.

Thorndike et al. [1975] presented a governing equation for the thickness distribution of sea ice:

$$\frac{\partial g}{\partial t} = -\nabla \cdot (\mathbf{v}g) - \frac{\partial}{\partial h}(fg) + \psi, \tag{1}$$

where h is the ice thickness; $\mathbf{v}$ is the horizontal velocity; $f = dh/dt$ is the thermodynamic growth rate; ψ is a function describing the redistribution of ice due to convergence, divergence, and shear; and $g(\mathbf{x}, h, t)$ is the thickness distribution function, with $g\,dh$ defined as the fractional area covered by ice whose thickness lies between h and $h + dh$. Note that $\int_0^\infty g\,dh = 1$ by definition. Equation (1) can be solved to a reasonable approximation by splitting it into three pieces and solving each in turn. For example, $\partial g/\partial t = -\nabla \cdot (\mathbf{v}g)$ is solved using a two-dimensional transport scheme, and $\partial g/\partial t = \psi$ is solved using a ridging model. This paper is primarily concerned with the remaining equation, which describes the transport of g in thickness space as ice grows and melts:

$$\frac{\partial g}{\partial t} = -\frac{\partial}{\partial h}(fg), \tag{2}$$

where g depends on h and t at a given location x.

Equation (2) has the same form as the one-dimensional fluid transport or continuity equation:

$$\frac{\partial \rho}{\partial t} = \frac{-\partial}{\partial x}(\rho u), \tag{3}$$

where ρ is the fluid density and u is the horizontal velocity. There are two general approaches to solving this equation. One is to discretize it as a finite difference equation and step the solution forward in time. The other, known as remapping [*Dukowicz and Baumgardner*, 2000], relies on the fact that (3) is mathematically equivalent to a mass conservation equation,

$$\frac{d}{dt}\int_{x_L(t)}^{x_R(t)} \rho\, dx = 0, \tag{4}$$

where $x_L(t)$ and $x_R(t)$ are the boundaries of a Lagrangian volume. That is, x_L and x_R follow the fluid motion and always enclose the same material particles. Thus, if the cell boundaries are projected forward in time from t^j to t^{j+1}, the mean densities $\bar{\rho}^{j+1}$ of the displaced cells are given by

$$\bar{\rho}^{j+1}(x_R^{j+1} - x_L^{j+1}) = \bar{\rho}^j(x_R^j - x_L^j). \tag{5}$$

Given the new mean densities, the density field can be reconstructed on the displaced grid and then interpolated, or remapped, onto the original grid. The accuracy of the method depends on the accuracy of the reconstruction. It is straightforward to design a one-dimensional remapping scheme that is second-order accurate in space. The time step is not limited by a stability criterion, as in finite difference schemes, but only by

Paper number 2000JC000518.

the requirement that fluid trajectories in neighboring grid cells do not cross.

The similarity of (2) and (3) suggests that remapping could be applied to the ice thickness distribution. Assume there are N discrete thickness categories, each with fractional area c_n, mean ice thickness h_n, left boundary H_{n-1}, and right boundary H_n. Open water is represented by a category with area c_0 at $h = 0$. The category boundaries form a one-dimensional grid on which g can be discretized. The ice area in category n is

$$c_n = \int_{H_{n-1}}^{H_n} g \, dh \tag{6}$$

and is conserved following the motion through thickness space:

$$\frac{dc_n}{dt} = 0, \tag{7}$$

where

$$\frac{d}{dt} \equiv \frac{\partial}{\partial t} + f\frac{\partial}{\partial h} \tag{8}$$

is the material derivative and the growth rate f is the analogue of velocity in thickness space. The ice volume is

$$v_n \equiv c_n h_n = \int_{H_{n-1}}^{H_n} hg \, dh. \tag{9}$$

The volume tendency following the motion is given by

$$\frac{dv_n}{dt} = c_n f_n, \tag{10}$$

where $f_n \equiv dh_n/dt$ is the thermodynamic growth rate in category n. Equations (6)–(10) form the basis for a scheme of remapping ice area and volume.

Section 2 reviews other methods that have been used to solve (2), each of which has certain disadvantages. Section 3 describes a more accurate method: a remapping scheme similar to that developed by *Dukowicz and Baumgardner* [2000] for spatial transport. Section 4 applies this scheme to two test problems with exact solutions, and the results are compared to the "fixed thickness" method of *Hibler* [1980] and the "delta function" method of *Bitz et al.* [2001]. Section 5 tests the remapping scheme, along with the fixed thickness and delta function schemes, in a single-column sea ice model with forcing typical of the central Arctic. Section 6 gives conclusions.

2. Other Solution Methods

Thorndike et al. [1975] were the first to solve (2) in sea ice models. In their scheme, there are N thickness categories, each with a prescribed mean thickness h_n. Given fractional ice areas c_n at time t, temporary thicknesses h_n^* at time $t + \Delta t$ are computed with a thermodynamic ice model, holding the areas fixed. Area is then transferred between neighboring categories so as to restore the thickness to h_n in each category while conserving total ice area. This is done by defining a function $G(h)$ equal to the fractional area of ice with thickness less than or equal to h. Since the areas are unchanged by thermodynamics, we have $G_n(t) = G_n^*(t + \Delta t)$, where $G_n(t)$ is the area of ice with $h \le h_n$ at time t and $G_n^*(t + \Delta t)$ is the area of ice with $h \le h_n^*$ at $t + \Delta t$. We deduce $G_n(t + \Delta t)$, the area with $h \le h_n$ at $t + \Delta t$, by interpolating linearly between adjacent values of $G_n^*(t + \Delta t)$. The new fractional areas $c_n(t + \Delta t)$ are given by the differences $G_n(t + \Delta t) - G_{n-1}(t + \Delta t)$. This scheme conserves ice area but not volume. The new ice volume should be equal to the sum over categories of the products $c_n(t)h_n^*$, but in fact, it is equal to the sum of the products $c_n(t + \Delta t)h_n$. In general, these sums are not equal.

Hibler [1980] presented a finite difference scheme that conserves both area and volume. He showed that volume is conserved when transferring ice from category n to category m if the transferred area is given by

$$\Delta c_{nm} = \frac{c_n f_n \Delta t}{h_m - h_n}, \tag{11}$$

where f_n is the growth rate in category n and h_m and h_n are fixed mean thicknesses. When f_n is positive, $m = n + 1$, and when f_n is negative, $m = n - 1$. The thinnest and thickest categories receive special treatment to ensure that no ice is thinner than h_1 or thicker than h_N. This scheme, like that of *Thorndike et al.* [1975], is first-order accurate in thickness space. It can be made second-order accurate by computing growth rates at the category boundaries instead of the mean thicknesses, but then volume is not conserved. Like many first-order schemes, this scheme is highly diffusive; peaks in the distribution quickly smear out over a broad range of thicknesses. Many categories are needed to converge to the solution of (2). *Flato and Hibler* [1995], for example, used 28 categories each of ridged and undeformed ice to limit diffusion and improve accuracy. For this reason Hibler's scheme may be too expensive for climate models, in which the computational cost of sea ice thermodynamics and horizontal transport increases linearly with the number of categories.

A third thickness distribution scheme assigns to each category an ice thickness that changes over time and is not constrained to lie between prescribed boundaries. When ice grows in open water, a new category is added temporarily. Then the two categories nearest in thickness or some related property are merged to keep the number of categories constant. *Bjork* [1992], *Schramm et al.* [1997], and *Lipscomb* [1998] used variations of this scheme, which is less diffusive and more accurate than Hibler's scheme. Model results generally converge with 5–10 categories. While this method is convenient for single-column ice models, it is unsuitable for three-dimensional models. The ice thickness h_n in one grid cell can differ substantially from the thickness in a neighboring cell, whereas two-dimensional transport schemes assume that h_n is uniform across the grid. Thus horizontal transport cannot be treated consistently.

A fourth method, tested extensively by *Bitz et al.* [2001], allows the thickness to vary in each category as ice grows and melts, but only within prescribed limits. Each category has a left boundary H_{n-1} and a right boundary H_n. When $h_n > H_n$, all the ice in category n moves to category $n + 1$, and when $h_n < H_{n-1}$, all the ice shifts to $n - 1$. During winter, ice growing in open water is added to category 1. In summer, when the ice is thinning, category 1 is reshaped as necessary, conserving volume, so that h_1 is never smaller than a prescribed minimum. H_N is chosen large enough that ice never outgrows the thickest category. This scheme is simple, inexpensive, com-

patible with horizontal transport, and not too diffusive. Bitz et al. found that about five categories are sufficient to represent the main effects of the thickness distribution on heat and freshwater fluxes. The major weakness of this solution method is that g is represented in each category as a delta function rather than a continuous finite distribution. Since ice is transferred between categories all at once instead of incrementally, properties of the thickness distribution such as the ice strength can change significantly in a single time step if g is not well resolved. Categories from which ice has recently been transferred often contain little ice, effectively reducing the resolution in thickness space.

Of these four methods, those of *Hibler* [1980] and *Bitz et al.* [2001] are the best suited for three-dimensional modeling since they conserve ice volume and are compatible with horizontal transport. Henceforth we refer to these methods as the fixed thickness and delta function schemes, respectively. The two schemes have complementary strengths and weaknesses. The fixed thickness scheme, while numerically smooth, is highly diffusive, and the delta function scheme, while nondiffusive, allows sharp numerical jumps.

The remapping scheme described below is both smooth and nondiffusive. It is similar to the scheme of *Thorndike et al.* [1975] in that the thickness distribution evolves onto a displaced grid before being remapped to the original grid. However, there are two key differences. First, h_n can vary over time in each category, although it remains between prescribed boundaries H_{n-1} and H_n. Second, g can vary with h within each category. (The scheme of Thorndike et al., in representing $G(h)$ as piecewise linear, implicitly assumes that g is constant within each category.) The result is a more accurate method that conserves ice volume.

3. Remapping the Thickness Distribution

We first describe the motion of category boundaries through thickness space, then show how to approximate g in each displaced category, and finally, show how to transfer ice area and volume to restore the original boundaries. Assume that at time j the ice areas c_n^j and mean thicknesses h_n^j are known for each of N thickness categories, with $N \geq 2$. Each category has a prescribed right boundary H_n. A thermodynamic model computes the new mean thicknesses h_n^{j+1} at time $j + 1$. The time step must be small enough that $h_n^{j+1} < h_{n+1}^{j+1}$ for each pair of adjacent categories. The growth rate at h_n is given by $f_n = (h_n^{j+1} - h_n^j)/\Delta t$. By linear interpolation we estimate the growth rate F_n at H_n:

$$F_n = f_n + \frac{f_{n+1} - f_n}{h_{n+1} - h_n}(H_n - h_n). \tag{12}$$

If c_n or $c_{n+1} = 0$, F_n is set to the growth rate in the nonzero category, and if $c_n = c_{n+1} = 0$, we set $F_n = 0$. The temporary displaced boundaries for $n = 1$ to $N - 1$ are given by $H_n^* = H_n + F_n \Delta t$. In principle, the boundaries can shift by arbitrary distances, but the method is easier to implement if the displaced boundaries satisfy $H_{n-1} < H_n^* < H_{n+1}$.

The ice areas in the displaced categories are $c_n^{j+1} = c_n^j$ since area is conserved following the motion, and the ice volumes are therefore $v_n^{j+1} = c_n^j h_n^{j+1}$. For simplicity we define $H_L = H_{n-1}^*$ and $H_R = H_n^*$ and drop the superscript $j + 1$. We wish to construct a continuous function $g(h)$ within each category such that (6) and (9) are satisfied. The simplest polynomial that can satisfy both equations is a line. It is convenient to change coordinates, writing $g(\eta) = g_1 \eta + g_0$, where $\eta = h - H_L$ and the coefficients g_1 and g_0 are to be determined. Then (6) and (9) can be written as

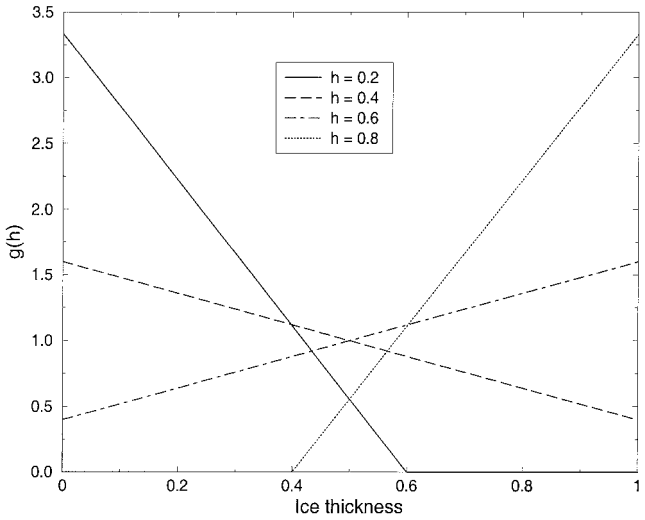

Figure 1. Linear reconstruction of the thickness distribution function $g(h)$ for an ice category with left boundary $H_L = 0$, right boundary $H_R = 1$, fractional area $c_n = 1$, and mean ice thickness $h_n = 0.2$, 0.4, 0.6, and 0.8.

$$\begin{aligned} g_1 \frac{\eta_R^2}{2} + g_0 \eta_R &= c_n \\ g_1 \frac{\eta_R^3}{3} + g_0 \frac{\eta_R^2}{2} &= c_n \eta_n, \end{aligned} \tag{13}$$

where $\eta_R = H_R - H_L$ and $\eta_n = h_n - H_L$. Equation (13) has the solution

$$\begin{aligned} g_1 &= \frac{12 c_n}{\eta_R^3}\left(\eta_n - \frac{\eta_R}{2}\right) \\ g_0 &= \frac{6 c_n}{\eta_R^2}\left(\frac{2\eta_R}{3} - \eta_n\right). \end{aligned} \tag{14}$$

Since g is linear, its maximum and minimum values lie at the boundaries, $\eta = 0$ and η_R:

$$\begin{aligned} g(0) &= \frac{6 c_n}{\eta_R^2}\left(\frac{2\eta_R}{3} - \eta_n\right) = g_0 \\ g(\eta_R) &= \frac{6 c_n}{\eta_R^2}\left(\eta_n - \frac{\eta_R}{3}\right). \end{aligned} \tag{15}$$

Equation (15) implies that $g(0) < 0$ when $\eta_n > 2\eta_R/3$, i.e., when h_n lies in the right third of the thickness range (H_L, H_R). Also, $g(\eta_R) < 0$ when $\eta_n < \eta_R/3$, i.e., when h_n falls in the left third of the range. Since negative values of g are unphysical, a different solution is needed whenever h_n lies outside the central third of the thickness range. If h_n is in the left third of the range, we define a cutoff thickness, $H_C = 3h_n - 2H_L$, and set $g = 0$ between H_C and H_R. Equation (14) is then valid with $\eta_R = H_C - H_L$. Similarly, if h_n is in the right third of the range, we define $H_C = 3h_n - 2H_R$ and set $g = 0$ between H_L and H_C. In this case, (14) applies with $\eta_R = H_R - H_C$ and $\eta_n = h_n - H_C$. If $g = 0$ in the part of a category that is remapped to a neighboring category, no ice is transferred.

Figure 1 illustrates the linear reconstruction of g for the simple cases $H_L = 0$, $H_R = 1$, $c_n = 1$, and $h_n = 0.2$, 0.4,

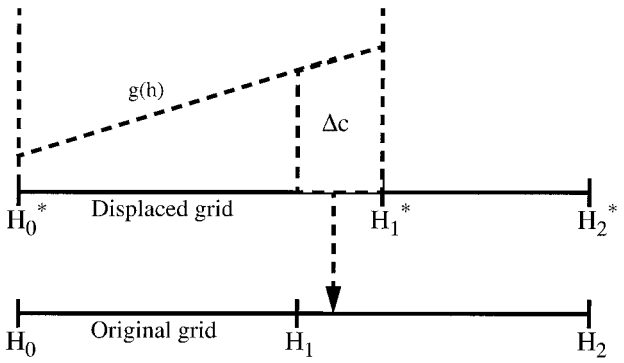

Figure 2. Transfer of ice area from category 1 to category 2 when ice is growing in category 1. The transferred area Δc is equal to the area under $g(h)$ between the original and displaced boundaries. The transferred volume (not shown) is equal to the area under $hg(h)$ between the original and displaced boundaries.

0.6, and 0.8. Note that g slopes downward when h_n is less than the midpoint thickness $(H_L + H_R)/2$ and upward when h_n exceeds the midpoint thickness. For $h_n = 0.2$ and 0.8, $g = 0$ over part of the range. Zero values are aesthetically displeasing and physically unrealistic for categories in the middle of the thickness distribution. In practice, however, h_n usually falls in the central third of the thickness range when categories $n - 1$ and $n + 1$ contain significant amounts of ice. Often, $g = 0$ in part of a category when the adjacent category contains little or no ice. However, in these cases, zero values improve the simulation by eliminating diffusion.

This procedure for computing g is different from that of *Dukowicz and Baumgardner* [2000]. In the one-dimensional version of that scheme a continuous scalar function $\rho(x)$ constructed from the mean values $\bar{\rho}$ must satisfy a single equation:

$$\int_{x_L}^{x_R} \rho(x)\, dx = \bar{\rho}(x_R - x_L). \tag{16}$$

Setting $\rho(x) = \bar{\rho}$ gives a first-order accurate scheme. To obtain second-order accuracy, we set $\rho(x) = \rho_1 x + \rho_0$ using the extra degree of freedom to match the slope of ρ in cell n to the slope of the line joining $\bar{\rho}_{n-1}$ and $\bar{\rho}_{n+1}$. When we construct a thickness distribution function $g(h) = g_1 h + g_0$, we must satisfy two equations. The mean of g is determined by the area equation (6), and the slope is determined by the volume equation (9). We cannot adjust the slope on the basis of the mean of g in neighboring categories.

We could aim for greater accuracy by approximating g as a quadratic polynomial $g_2 h^2 + g_1 h + g_0$ and imposing a curve-fitting constraint similar to that of *Dukowicz and Baumgardner* [2000]. A reasonable constraint is to minimize the least squares difference between g and the quadratic polynomial γ passing through the mean values of g in categories $n - 1$, n, and $n + 1$. That is, we minimize the quantity

$$\lambda \equiv \int_{H_L}^{H_R} [\, g(h) - \gamma(h)]^2\, dh \tag{17}$$

by computing the roots of $d\lambda/dh$. This procedure is algebraically complex but yields a unique best fit g. If $g < 0$ over part of the range, we can find an alternative g that satisfies (6) and (9) and is nonnegative over the range. Since it is not obvious that the quadratic scheme is significantly more accurate than the linear scheme, we test both schemes in sections 4 and 5.

After constructing g in each displaced category we remap the thickness distribution to the original boundaries by transferring area and volume among categories. We need to compute the ice area Δc_n and volume Δv_n between each original boundary H_n and displaced boundary H_n^*. If the boundary has shifted to the right, ice moves from category n to $n + 1$. The area and volume transferred are

$$\Delta c_n = \int_{H_n}^{H_n^*} g\, dh$$
$$\Delta v_n = \int_{H_n}^{H_n^*} hg\, dh. \tag{18}$$

If the boundary has moved to the left, ice area and volume are transferred from $n + 1$ to n using (18) with the limits of integration reversed. It is straightforward to change coordinates to $\eta = h - H_L$, where H_L is the left limit of the range over which $g > 0$. Thus we obtain the new areas c_n and volumes v_n between the original boundaries H_{n-1} and H_n for each category. The new thicknesses $h_n = v_n/c_n$ are guaranteed to lie between the appropriate boundaries. This procedure is illustrated in Figure 2 for the simple case $N = 2$, with ice growing in category 1.

Other conserved quantities are transferred in proportion to the ice volume Δv_i. (Here we drop the subscript n and use the subscripts i and s to distinguish between ice and snow variables.) The transferred snow volume is $\Delta v_s = v_s(\Delta v_i/v_i)$, where $v_s = ch_s$. Given the new ice area and snow volume, the new snow thickness is $h_s = v_s/c$. The enthalpy q_i, defined as the energy needed to melt a unit volume of ice, is treated similarly. Let v_{ik} denote the ice volume in layer k. Defining the ice energy in layer k as $e_{ik} = v_{ik}q_{ik}$, we have $\Delta e_{ik} = e_{ik}(\Delta v_i/v_i)$. From the new values of e_{ik} and v_{ik} we compute the new enthalpies $q_{ik} = e_{ik}/v_{ik}$. Other state variables are treated analogously.

The left and right boundaries of the domain require special treatment. If ice is growing in open water at a rate F_0, the left boundary $H_0 = 0$ is shifted to the right by $F_0\Delta t$ before g is constructed in category 1, then reset to zero after the remapping is complete. New ice is then added to category 1, conserving area, volume, and energy. If ice cannot grow in open water (because the ocean is too warm or the net surface energy flux is downward), H_0 is fixed at zero, and the growth rate at the left boundary is estimated as $F_0 = f_1$. The area of ice thinner than $\Delta h_0 = -F_0\Delta t$ is added to the open water area c_0, leaving the ice and snow volume and energy unchanged. This area is given by

$$\Delta c = \int_0^{\Delta h_0} g\, dh. \tag{19}$$

The right boundary H_N varies with h_N. If g is linear, we set $H_N = 3h_N - 2H_{N-1}$, which ensures that $g(H_N) = 0$. For the quadratic case we set $H_N = 4h_N - 3H_{N-1}$, which guar-

antees in addition that $\partial g/\partial h = 0$ at H_N. No ice crosses this boundary.

4. Two Test Problems With Exact Solutions

We now apply the linear and quadratic remapping schemes, along with the fixed thickness and delta function schemes, to two simple test problems with exact solutions. For both problems the ice is confined to the interval (0, 1), which is divided into N categories of equal width. The resolution is alternated between $N = 5$ and $N = 10$. All quantities are dimensionless.

For the first problem the thickness distribution at $t = 0$ is a "top hat": $g = 5$ for $0 < h < 0.2$, and $g = 0$ elsewhere. This distribution moves to the right with uniform velocity $f = 1$. To obtain numerical solutions, we initialize each category with the same ice area and mean thickness as in the exact problem. That is, the five-category simulations begin with $c = 1$ and $h = 0.1$ in category 1 and $c = 0$ in categories 2–5. The 10-category simulations start with $c = 0.5$ and $h = 0.5$ in category 1, $c = 0.5$ and $h = 0.15$ in category 2, and $c = 0$ in categories 3–10. The solution is then marched forward with time step $\Delta t = 10^{-3}$. (Decreasing Δt does not change the results significantly.) We first compute the ice growth in each category, $\Delta h_n = f\Delta t$, and then transfer ice area and volume as prescribed by the scheme being tested.

Figure 3 shows the solutions at $t = 0.4$, when the exact solution is a top hat with $g = 5$ for $0.4 < h < 0.6$ and $g = 0$ elsewhere. The thickness distribution in each category is represented by a flat line segment for the fixed thickness scheme, a sloped line segment for linear remapping, and a curved segment for quadratic remapping. For the delta function scheme, g is represented by a vertical line at $h = h_n$; the height of the line is equal to the mean value of g in the category, $\bar{g} = c_n/(H_n - H_{n-1})$. (We cannot plot g itself because it is infinitely tall and thin.) The delta function scheme

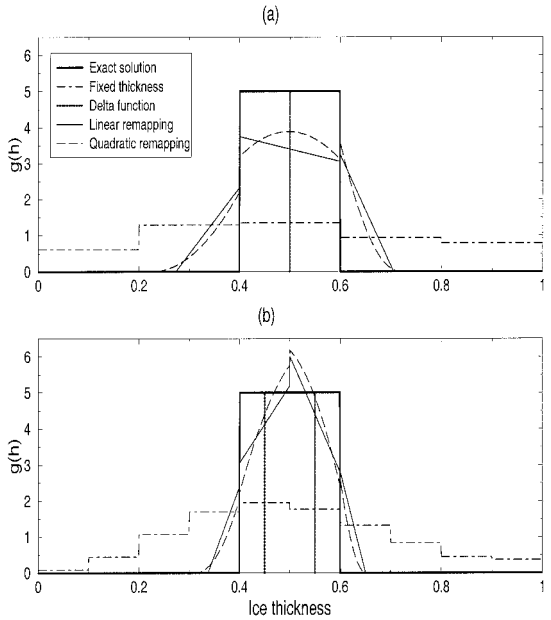

Figure 3. Comparison of exact to numerical solutions with initial condition $g = 5$ for $0 < h < 0.2$ and $g = 0$ elsewhere: (a) 5 thickness categories and (b) 10 thickness categories. The initial top hat distribution moves uniformly to the right until centered at $h = 0.5$.

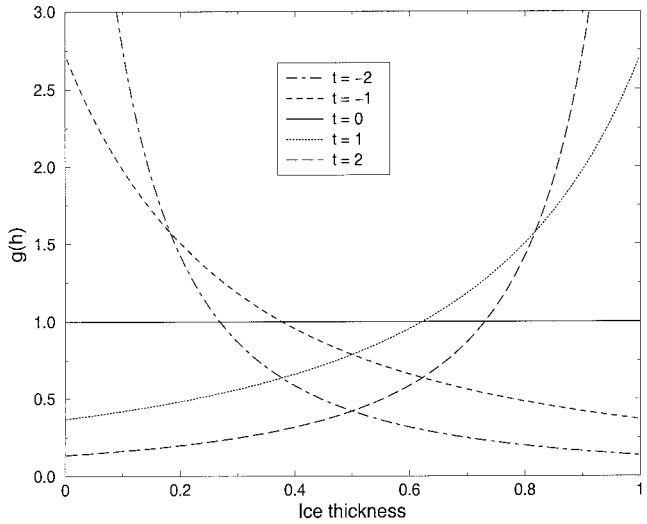

Figure 4. Exact solution to (2) at five different times given parabolic growth rate $f(h) = h - h^2$ and initial condition $g(h, 0) = 1$ for $0 < h < 1$. The solution is symmetric in time about $t = 0$.

behaves perfectly for this problem. For $N = 5$ all the ice lies in category 3, with mean thickness $h_3 = 0.5$, and for $N = 10$ the ice is divided equally between categories 5 and 6, with h_n centered in each category. The remapping schemes give the next best solutions. The thickness distribution is not perfectly symmetric about $h = 0.5$, nor is it confined to the central interval (0.4, 0.6), but it is still sharply peaked. With $N = 5$ the linear scheme permits 32% of the ice area to drift outside the central interval, compared to 27% for the quadratic scheme. For $N = 10$ these errors fall to 15 and 11%, respectively. The fixed thickness solutions are extremely diffuse; the area outside the central interval is 73% for $N = 5$ and 63% for $N = 10$.

The delta function scheme is ideal for narrowly peaked distributions. Real distributions, however, are usually spread out over a range of thicknesses. Thus we solve a second test problem in which the growth rate is $f(h) = h - h^2$, so that $f > 0$ for $0 < h < 1$ and $f = 0$ at the boundaries. This is not a realistic ice growth rate, but it permits an exact solution of (2). Suppose that at $t = 0$ we have $g(h) = 1$ for $0 < h < 1$ and $g(h) = 0$ elsewhere. Then the general solution is

$$g(h,t) = \frac{e^t}{[e^t(1-h) + h]^2}. \tag{20}$$

This solution is symmetric in time about $t = 0$ and is shown in Figure 4 for five values of t. Ice accumulates near $h = 0$ as $t \to -\infty$ and near $h = 1$ as $t \to \infty$. Total area is conserved. To obtain numerical solutions, we initialize c_n and h_n at $t = -1$ by integrating (20) between category boundaries, using (6) and (9). For the fixed thickness scheme the initial volumes differ slightly from the exact values since the mean thicknesses are prescribed, but the initial areas are the same. The solution is stepped forward with $\Delta t = 10^{-3}$.

The resulting thickness distributions are shown in Figure 5 for $t = 0$ and Figure 6 for $t = 1$. Since linear and quadratic remapping give nearly identical distributions, the quadratic solutions are not shown. First, consider the solutions at $t = 0$. Linear remapping gives by far the best solutions. With $N = 5$ (Figure 5a) the rms deviation between the computed and exact

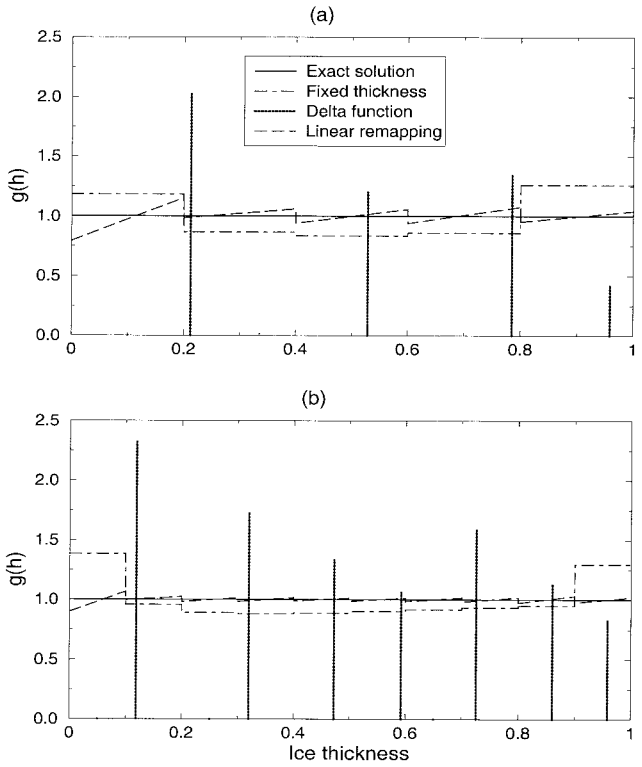

Figure 5. Comparison of exact to numerical solutions at $t = 0$ with a parabolic growth rate: (a) 5 thickness categories and (b) 10 thickness categories. The numerical experiments are initialized at $t = -1$.

solutions is just 0.056, with a maximum deviation of 0.20 at the left boundary. The fixed thickness scheme puts too much ice near the boundaries and too little in the interior, resulting in an rms deviation of 0.18. The delta function scheme has too little ice in category 5 and no ice at all in category 1, which has merged with category 2. With $N = 10$ (Figure 5b) the linear remapping solution has improved further. The rms deviation has fallen by a factor of 3 to 0.019, with a maximum deviation of 0.10. The fixed thickness scheme again diffuses ice toward the boundaries, and the rms deviation has fallen only to 0.17. In the delta function solution, only seven categories remain, with widely scattered values of g.

In Figure 6, for $t = 1$, linear remapping again gives the best solutions. The rms deviations are 0.068 for $N = 5$ and 0.025 for $N = 10$. The fixed thickness scheme again puts too much ice near the boundaries, and the rms deviation decreases only slightly, from 0.31 to 0.30, as N increases from 5 to 10. The delta function scheme allows more categories to disappear as the system evolves; only 3 of the original 5 categories remain in Figure 6a, and 5 of 10 in Figure 6b.

These results suggest that remapping is the best method for solving (2). For sharply peaked distributions it is less accurate than the delta function scheme but is reasonably nondiffusive, unlike the fixed thickness scheme. For broader distributions, remapping is much more accurate than the other schemes, without the loss of resolution associated with category mergers in the delta function scheme. Since linear and quadratic remapping give similar results, the added complexity of quadratic remapping seems unnecessary. Linear remapping appears to be roughly second-order accurate in thickness space, although it is not possible to prove this formally as with finite difference schemes.

5. Remapping in a Single-Column Sea Ice Model

The test problems of section 4 are very simple, with unrealistic ice growth functions and no thermodynamic or dynamic feedbacks. Therefore we also test the various schemes in a more realistic model. There is no exact solution to which model results can be compared; the best we can do is increase the number of thickness categories until the solution converges and assume that the asymptotic solution is close to the "true" solution. The excellent performance of the remapping schemes in the two test cases provides some confidence that this assumption is valid.

5.1. Model Description

The sea ice model used for these tests is a single-column model with thermodynamics and ridging but without full-fledged dynamics and horizontal transport. That is, the first term on the right side of (1) is neglected, but the redistribution function ψ, which ridges thin ice into thick ice, is included. Neglecting the two horizontal dimensions considerably simplifies the analysis. The model is forced with temperatures and fluxes typical of the central Arctic, where the thickness distribution is most important.

For each thickness category a thermodynamic model computes growth and melting at the top and bottom surfaces along with changes in internal ice and snow temperatures. The model is similar to those described by *Lipscomb* [1998] and *Bitz and*

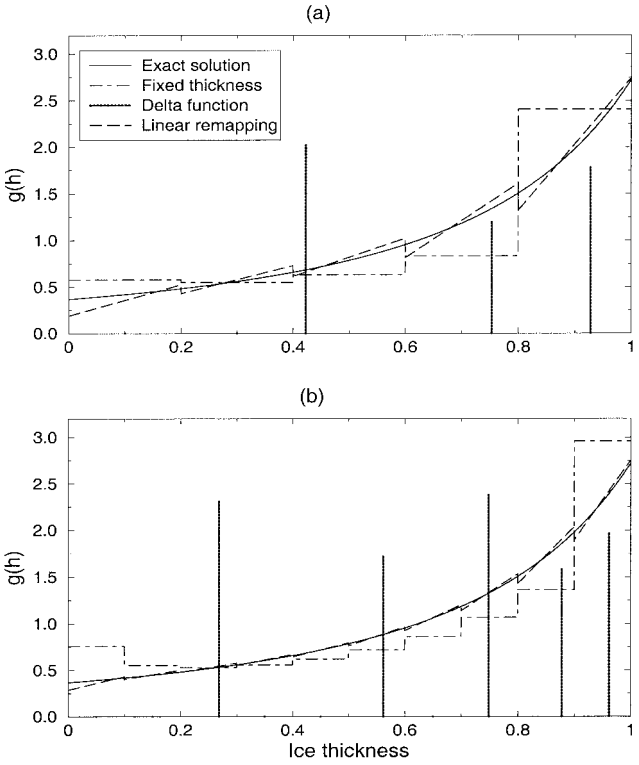

Figure 6. Comparison of exact to numerical solutions at $t = 1$ with a parabolic growth rate: (a) 5 thickness categories and (b) 10 thickness categories. As in Figure 5, the numerical solutions are initialized at $t = -1$.

Lipscomb [1999]. As in the model of *Maykut and Untersteiner* [1971], the heat capacity of sea ice depends on temperature and salinity and becomes large as the temperature approaches 0°C. The ice salinity profile is prescribed and increases from 0 ppt at the top surface to 3.2 ppt at the bottom. There are four internal ice layers and a single snow layer. The top surface temperature is found by requiring that the sum of radiative, turbulent, and conductive fluxes is zero, unless this would yield $T_{sfc} > 0$°C, in which case T_{sfc} is fixed at 0°C and ice melts. Ice can grow or melt at the bottom surface, which is fixed at the freezing temperature of seawater, $T_f = -1.8$°C.

The surface albedo depends on the surface type, temperature, and thickness, and thus varies among the categories. The albedo of snow is 0.85 when $T_{sfc} < 0$°C and 0.75 when $T_{sfc} = 0$°C. The albedo of snow-free ice of thickness h_n is given by

$$\alpha_i = \alpha_{\min} + (\alpha_{\max} - \alpha_{\min})[1 - \exp(-h_n/h_\alpha)], \quad (21)$$

which models the observed increase of ice albedo with thickness. The maximum ice albedo, $\alpha_{\max} = 0.60$, represents an average over pond-covered and pond-free ice. The minimum, $\alpha_{\min} = 0.20$, is a typical value for very thin ice. The e-folding scale h_α is set to 50 cm. This scale is approximate; while the extreme values of ice albedo are reasonably well known [*Perovich et al*., 1999], there are few measurements of the variation of albedo with thickness.

The ice categories interact with an ocean mixed layer whose temperature T_{ml} is updated at each time step. The mixed layer exchanges energy with the atmosphere in areas of open water and absorbs solar radiation that penetrates beneath the ice. If $T_{ml} > T_f$, the ocean transfers heat to the bottom ice surface, following *Maykut and McPhee* [1995]. If $T_{ml} < T_f$, new ice grows in open water. T_{ml} is then reset to T_f, and the new ice is added to category 1.

The ridging model is based on *Thorndike et al*. [1975] and *Hibler* [1980]. It converts thin ice to thick ice, reducing the ice area while conserving ice volume and energy. In order to conserve total area the ice area lost during ridging is replaced by an equal area of open water. Hibler's parameter H^*, which determines the ridge thickness, is set to 25 m instead of 100 m to give better agreement with observed thickness distributions.

In three-dimensional models the ridging rate depends on the rates of convergence and shear. In a column model these rates are not computed, so we adopt the parameterization $R_{\text{net}} = R_0\exp(-P/P_0)$, where R_{net} is the net rate of area loss due to ridging of ice and closing of open water, P is the ice strength under compression, and R_0 and P_0 are tuned to give reasonable ridging rates. Following *Rothrock* [1975], P is proportional to the change in potential energy per unit area of compressive deformation. The values $R_0 = 2.0 \times 10^{-3}$ d^{-1} and $P_0 = 80$ kN m^{-1} give ridging rates in reasonable agreement with observations [*Vinje et al*., 1998] and models [*Flato and Hibler*, 1995].

Ice area is replaced by open water at a constant rate E to simulate export through Fram Strait. E is set to 5% yr^{-1} in order to obtain a mean ice thickness of just under 3 m, in agreement with observations [*Bourke and Garrett*, 1987; *Vinje et al*., 1998]. This value is lower than the observed export rate of about 10% yr^{-1} [*Kwok and Rothrock*, 1999].

The model is forced at the top surface with climatological values of the downward shortwave and longwave fluxes, air temperature, relative humidity, wind speed, and snowfall rate [*Lindsay*, 1998]. The climatology is based on measurements from Soviet drifting stations on perennial Arctic ice. Instantaneous values are computed by cubic interpolation from monthly means. The sensible and latent heat fluxes are derived from bulk parameterizations, following *Maykut* [1982].

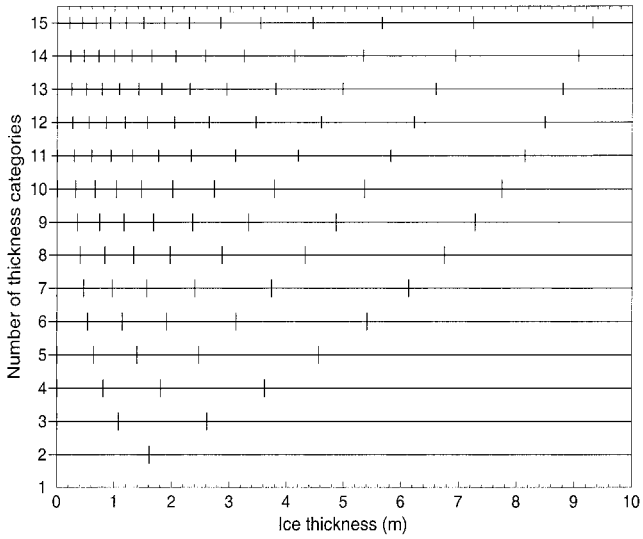

Figure 7. Thickness category boundaries for the single-column model as a function of the number of categories.

5.2. Model Results

We now evaluate the linear and quadratic remapping schemes, the fixed thickness scheme, and the delta function scheme using the single-column model. All experiments are initialized on January 1 with zero ice thickness and run for 100 years (long enough to reach steady state) with a 4 hour time step. For each scheme the number of categories N is varied from 1 to 15. Category boundaries are given by

$$H_n = H_{n-1} + c_1 + c_2\left\{1 + \tanh\left[c_3\left(\frac{n-1}{N} - 1\right)\right]\right\}, \quad (22)$$

with $H_0 = 0$, $c_1 = 3/N$, $c_2 = 15c_1$, and $c_3 = 3$. Like the formula used by *Hibler* [1980], this formula gives boundaries that are spaced more widely as n increases. Figure 7 shows the category boundaries for $N = 1$ to 15.

Figure 8 shows the annual mean ice thickness $\bar{h}$ in year 100 with standard forcing for each scheme. Figure 9 gives other results for year 100: (a) the annual mean net radiative/turbulent flux F_0 from the surface to the atmosphere, (b) the annual mean heat flux F_w from the ocean to the ice, (c) the annual thickness range, defined as the difference between the winter maximum and summer minimum values of the average ice thickness, and (d) the maximum ice strength. First, note the differences between single and multiple thickness categories. For $N = 1$ the four schemes are trivially equivalent, and the mean thickness, 2.61 m, is reasonably close to the asymptotic value of about 2.9 m. There are large errors, however, in the fluxes and ice strength. Since there is no thin ice to melt in summer, the ocean absorbs little sunlight, and $F_w = 0.6$ W m^{-2}, far below the asymptotic value of 2.9 W m^{-2}. Bottom melting is minimal, and the annual thickness range is 0.59 m, much less than the asymptotic value of 0.80 m. The maximum ice strength for $N = 1$ (not shown) is 330 kN m^{-1}, much greater than the asymptotic value of about 90 kN m^{-1}. As a result, the area of ice ridged is just 0.03 yr^{-1}, an order of magnitude less than the

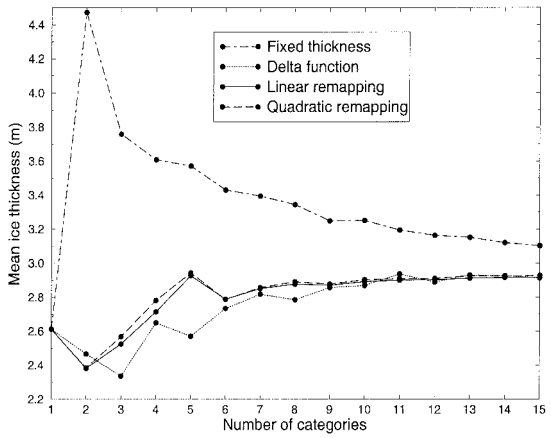

Figure 8. Variation of the annual mean ice thickness with the number of thickness categories for the four thickness distribution schemes. In each experiment the model is run for 100 years with standard forcing.

asymptotic value of 0.34. (A parameterization tuned for single-category models would give more reasonable values for ice strength and ridging.) These differences illustrate the need for multiple thickness categories.

Linear and quadratic remapping give nearly identical results. The mean thicknesses agree to within 7 cm for all N and to within 2 cm for $N \geq 5$. As N increases, both methods quickly converge to a mean thickness of just over 2.9 m. The mean thickness lies within 12 cm of the asymptotic value for $N \geq 5$ and within 6 cm of this value for $N \geq 7$. The fluxes and ice strength also converge rapidly. As N increases from 7 to 15, F_0 and F_w change by <0.05 W m^{-2}. The maximum ice strength varies by <5 kN m^{-1}, the annual area ridging varies by <0.01, and the thickness range varies by <1 cm. These results suggest that seven categories are sufficient for climate modeling. Five categories are adequate if we accept errors of 0.1 W m^{-2} in the surface fluxes, 10 kN m^{-1} in the ice strength, and 2 cm in the thickness range.

The delta function method is slower to converge. For $N = 5$–8 the mean thickness is 15–30 cm too low, mainly because of excessive summer melting. For $N > 10$ the surface fluxes and thickness range are close to the values given by remapping and do not vary much with N. The ice strength, however, is highly variable and generally exceeds the strength given by remapping.

The fixed thickness solutions differ markedly from the other solutions and converge very slowly. The mean thickness is 3.57 m for $N = 5$ and does not fall below 3 m until $N = 25$. This poor performance results from numerical diffusion, which broadens the thickness distribution and causes the ice to grow too quickly in winter and melt too quickly in summer. Since the excess winter growth outweighs the excess summer melt, $\bar{h}$ is too large. Winter growth is overestimated because growth rates are inversely proportional to ice thickness. Thus a broad distribution grows faster than a sharply peaked distribution with the same mean because fast growth to the left of the peak outweighs slower growth to the right. Excessive summer melt results from albedo feedback. Ice that diffuses into the thin end of the range melts quickly in summer, exposing open water and increasing solar absorption. The maximum open water area in the fixed thickness scheme is 0.195 for $N = 5$ and 0.143 for $N = 15$, compared to 0.102 and 0.096, respectively, for linear remapping. Thus F_w in the fixed thickness scheme is too large by 0.6–1.2 W m^{-2}, and there is too much bottom melting. Although the ice pack is too thick on average, it contains too much thin ice, which leads to further errors. It is weak and ridges excessively. Also, the downward flux of sensible heat in winter is too small, resulting in a net upward heat flux that is too large by 0.1–0.2 W m^{-2}.

Figure 10 shows several thickness distributions resulting from the standard forcing. Figures 10a and 10b are annual mean distributions in year 100 for $N = 5$ and 15, respectively, and Figures 10c and 10d are snapshots of g at the end of December of year 100, again for $N = 5$ and 15. The open water fraction (not shown) is about 0.02 for the mean plots and is negligible for the December plots.

Consider first the remapping schemes. The linear and quadratic schemes give similar distributions in reasonable agreement with observations [*Vinje et al.*, 1998]. In each plot, g increases from a small value at $h = 0$ to a peak near 2 m, falls off sharply to the right of the peak, then declines more gradually at larger thicknesses. The thermodynamic peaks for $N = 15$ are sharper than typically observed, mainly because of the constant year-to-year forcing and the simple ridging scheme. For $N = 5$, g is set to zero in the thicker part of category 4. For $N = 15$, however, the distributions are smoother and do not go to zero. In December, 15 categories are enough to resolve a secondary peak of first-year ice about 1 m thick.

The fixed thickness distributions are broader with lower peaks. With $N = 15$, for example, the maximum values of g are 0.29 for the annual mean and 0.39 at the end of December, compared to 0.51 and 0.70 for linear remapping. These distributions resemble observations more closely than do the sharply peaked remapping plots. However, they are broad for

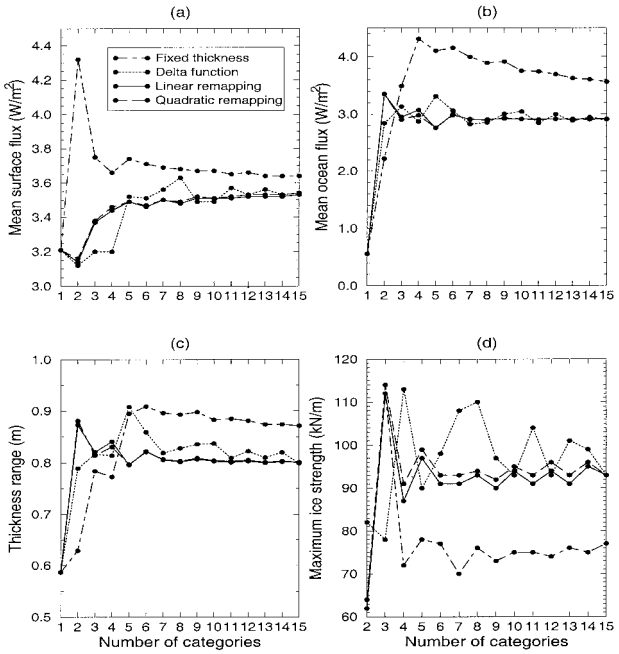

Figure 9. Variation of other quantities with the number of thickness categories (year 100, standard forcing): (a) annual mean radiative/turbulent flux from surface to atmosphere, (b) annual mean heat flux from ocean to ice, (c) annual range of mean ice thickness, and (d) maximum ice strength.

the wrong reason: not because of realistic variability in thermodynamics and ridging but because of numerical diffusion.

The delta function distributions have some irregular numerical properties. With $N = 5$, there is almost no ice in category 4 at the end of December. Figure 11a shows how the areas in categories 1–4 vary through the year. About 40% of the area shifts from category 3 to 4 in January, then back to category 3 in July, where it remains the rest of the year. About 35% of the area moves from category 2 to 3 in March, back to category 2 in July, and to category 1 in August; it then merges with new ice in September and returns to category 2 in November. At any given time, at least one category is nearly empty. With $N = 15$, five categories have fractional areas <0.01 at the end of year 100, including categories 6 and 10 in the heart of the distribution. Three other categories have areas <0.02. By comparison, remapping allows the category areas to vary smoothly in an intuitive way (Figure 11b). For $N = 15$ the fractional areas exceed 0.01 in categories 3–15 and are >0.05 in categories 5–13.

The delta function method also gives rise to multiyear variability, which is undesirable in a model forced identically each year. Figure 12a shows that for $N = 5$, $\bar{h}$ oscillates between 2.57 and 2.72 m over a 19 year cycle. This variability is associated with slow variations in the category areas, as illustrated in Figure 12b. Cycles arise because ice properties such as albedo and strength vary nonlinearly with thickness. Thus, when two categories merge, the combined category may have properties different from the mean properties of the two components. Figure 13 illustrates the discontinuity in ice strength when categories combine. In year 100 of the delta function simulation the ice strength jumps sharply when categories 1 and 2 merge in January and again in early March. In year 103, there is an additional increase when categories 2 and 3 combine in late March. No two consecutive years are alike. Since different values of N result in distinct cycles, properties such as the maximum ice strength in a given year may not converge with increasing N. For remapping, there are no such cycles; in steady state each year is virtually identical to the one before. The mean thickness is constant from year to year (Figure 12a), and the ice strength and other properties vary smoothly (Figure 13).

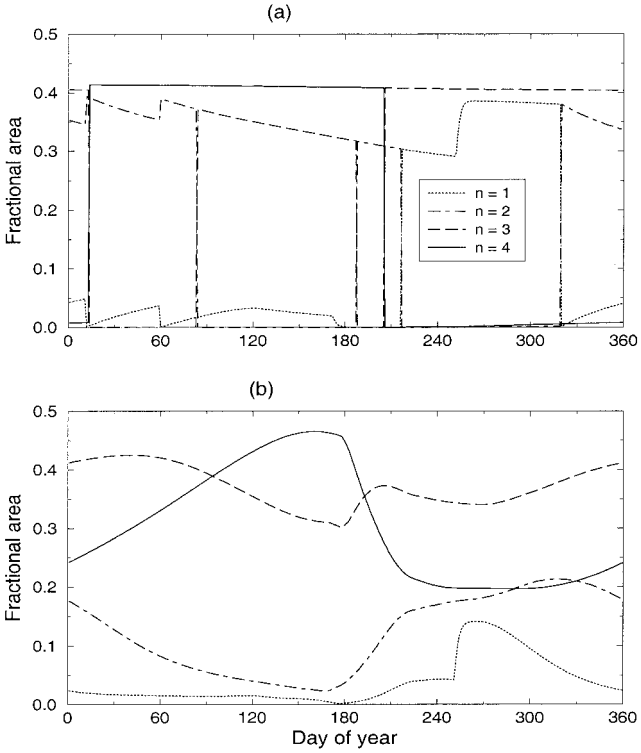

Figure 11. Variation of fractional area in categories 1, 2, 3, and 4 for $N = 5$ (year 100, standard forcing): (a) delta function scheme and (b) linear remapping.

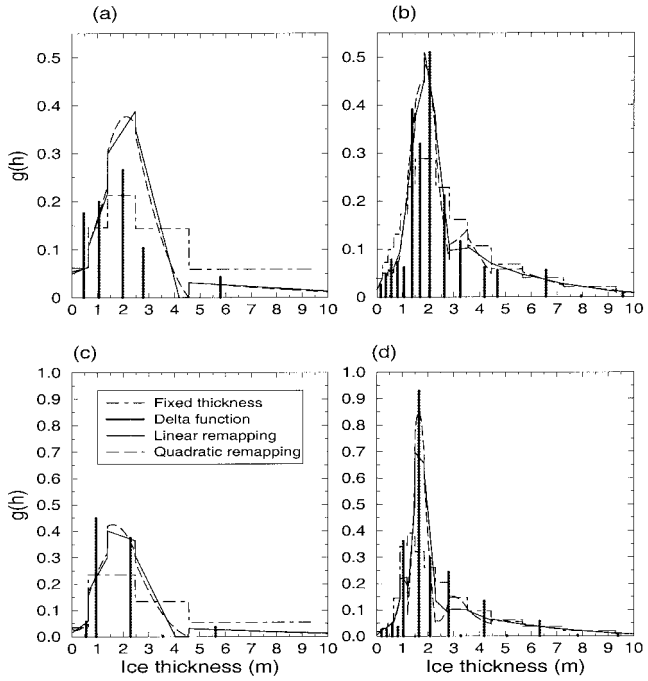

Figure 10. Ice thickness distributions in year 100 with standard forcing for the four schemes: (a) annual mean, $N = 5$; (b) annual mean, $N = 15$; (c) end of December, $N = 5$; and (d) end of December, $N = 15$. For the delta function scheme the mean value of g is plotted in each category.

Overall, the remapping methods outperform the other two methods with standard forcing. The fixed thickness scheme generates smooth thickness distributions but is less accurate and slower to converge. The delta function scheme is not too different from remapping for area-averaged annual mean quantities, but it behaves less well numerically and gives less realistic thickness distributions.

Remapping also performs well under modified forcing. Figure 14, for example, shows how the annual mean ice thickness in year 100 varies with N in two altered climates. In the "cold" climate the shortwave radiation is decreased by 5%, raising $\bar{h}$ to about 3.6 m (a 24% increase over the standard case), and in the "warm" climate the shortwave radiation is increased by 5%, lowering $\bar{h}$ to about 2.1 m (a 28% decrease). In both cases the fixed thickness method overestimates $\bar{h}$ and converges slowly, as with the standard forcing. Linear and quadratic remapping converge rapidly; for both climates, $\bar{h}$ lies within 8 cm of the asymptotic value for $N > 5$. The delta function method converges more slowly and generally underestimates the ice thickness.

The warm-climate solutions merit further discussion. At the beginning of summer the thickness distribution is sharply peaked around 1.6 m. The peak consists of first-year ice to-

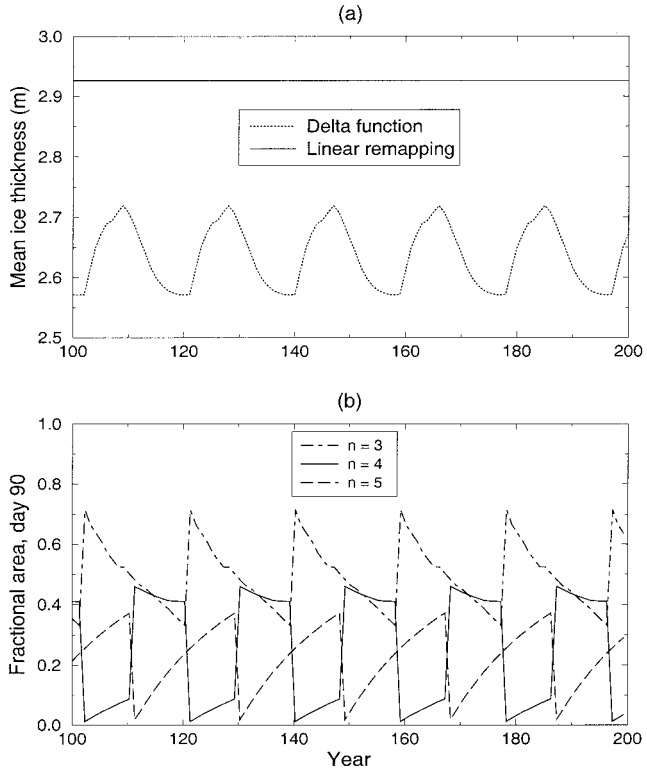

Figure 12. Multiyear variability for $N = 5$, years 100–200 with standard forcing: (a) annual mean ice thickness for the delta function and linear remapping schemes and (b) fractional area on day 90 in categories 3, 4, and 5 for the delta function scheme.

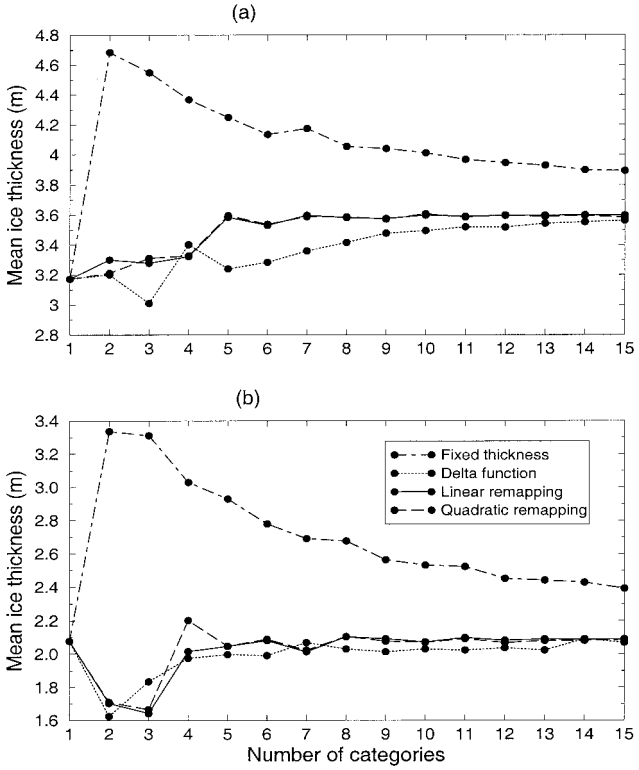

Figure 14. Variation of the annual mean ice thickness with the number of thickness categories during year 100 with modified forcing: (a) shortwave radiation decreased by 5% compared to standard forcing and (b) shortwave radiation increased by 5%.

gether with multiyear ice that nearly melted the previous summer. It is sharp because thin ice grows faster during the winter than thick ice, so that initially broad distributions tend to narrow. Figure 15 shows the evolution of this peak during the summer (days 180–250) with $N = 12$. For the delta function scheme (Figure 15a) more than half the ice cascades through the five thinnest categories, occupying only one category at a time. For the remapping scheme (Figure 15b) the peak spreads during the summer, so that by late summer the fractional area is 0.03 or more in each of categories 1–5. Equation (2) predicts

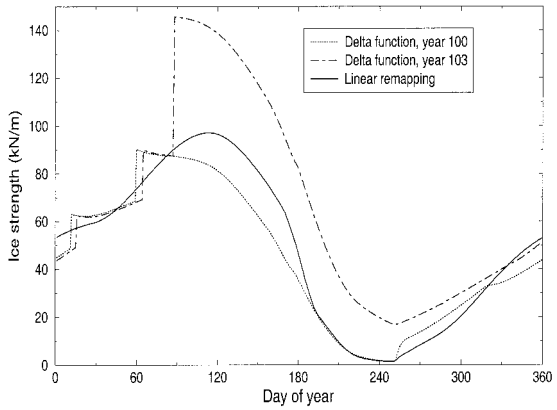

Figure 13. Variation of ice strength during the year with $N = 5$ and standard forcing for the delta function scheme (years 100 and 103) and linear remapping (year 100, which is nearly identical to all subsequent years).

that a narrow distribution should, indeed, spread during the summer provided that its initial width is finite and that thin ice melts faster than thicker ice (as it does). Thus the remapping scheme gives an increasingly accurate solution to (2) as N increases. The delta function scheme is less accurate because the initial peak is infinitely sharp and cannot spread. This scheme has a basic asymmetry; it can narrow a broad distribution when the velocities in thickness space are converging, but it cannot broaden a narrow distribution when the velocities are diverging.

Another interesting test is to set the ridging to zero. In this case the fraction of ice thicker than thermodynamic equilibrium, about 3 m, is a measure of model diffusivity. Figure 16a shows that $\bar{h}$ converges quickly with increasing N to about 2.8 m for the delta function and both remapping schemes. It is surprising that ridging has such a small effect on the mean ice thickness; the formation of thick ice is nearly balanced by the creation of open water. (Ridging would increase the mean thickness, however, in regions of strong net convergence.) As before, the fixed thickness scheme overestimates $\bar{h}$. Figure 16b shows the mean fractional area in each category during year 100 with $N = 10$. In a perfect model there would be no ice thicker than category 7, whose upper boundary is 3.78 m. The nondiffusive delta function scheme has a mean area of 0.56 in category 7 and zero in categories 8–10, as desired. The remapping schemes are less sharply peaked in category 7 and have small areas (0.07 and 0.06 for the linear and quadratic schemes, respectively) of 4 m ice near the left boundary of category 8, with no area in categories 9 and 10. Thus they are

mildly diffusive. The fixed thickness scheme is more diffusive, with a broad peak and a combined area of 0.29 in categories 8–10.

These simulations illustrate the main differences among the various schemes. The results are similar when the forcing varies from year to year, except that numerical variability in the delta function scheme is then harder to distinguish from natural variability. The linear remapping scheme has been implemented in the three-dimensional Los Alamos sea ice model, CICE [*Hunke and Lipscomb*, 1999], where it gives thickness distributions similar to those found in the column model.

6. Conclusions

The ice thickness distribution schemes tested to date in large-scale models have at least one of two major weaknesses. The fixed thickness scheme of *Hibler* [1980] is very diffusive; it requires 20–30 categories to converge accurately to the solution to (2). The delta function scheme of *Bitz et al.* [2001] is poorly behaved numerically; it allows discontinuous changes in ice properties that lead to spurious multiyear variability, and it leaves a substantial fraction of categories nearly empty at any given time. Remapping solves both problems. Since g is approximated in each thickness category as a linear or quadratic polynomial instead of a constant, remapping is more accurate and less diffusive than the fixed thickness scheme. Since ice moves between categories in small increments, remapping is smoother than the delta function scheme.

For these reasons, remapping significantly outperforms the alternative schemes. When applied to two complementary test problems, remapping gives excellent solutions that converge rapidly as the number of categories increases. The fixed thickness scheme is less accurate and slow to converge. The delta function scheme, while well suited for narrow distributions, gives poor results for broad distributions. In a more realistic single-column sea ice model the two remapping schemes again are more accurate and converge faster with increasing resolution than the other methods. The delta function method also converges fairly quickly in most cases, but its irregular numerical behavior limits its accuracy.

All these schemes are relatively inexpensive. The delta function scheme is the cheapest, followed by the fixed thickness scheme, linear remapping, and quadratic remapping. Linear remapping costs about 15% as much per category as the thermodynamic model used here, compared to 20% for quadratic remapping. With 10 or fewer categories the thermodynamic model is much cheaper than viscous plastic dynamics or second-order horizontal transport. Thus the cost of either remapping scheme in the context of a large-scale model is minimal.

Although quadratic remapping satisfies a curve-fitting constraint intended to increase its accuracy, it gives nearly the same results as linear remapping in all the cases studied. The area and volume equations, (6) and (9), constrain g enough that the additional constraint appears unnecessary. Since linear remapping is faster than quadratic remapping and simpler to implement, it is probably the better scheme for most applications, including climate modeling.

Several authors have tried to determine the minimum number of thickness categories needed to resolve the area-averaged annual cycles of ice thickness, ice strength, and surface fluxes. This study suggests that five to seven categories, with higher resolution for thinner ice, are sufficient. In column

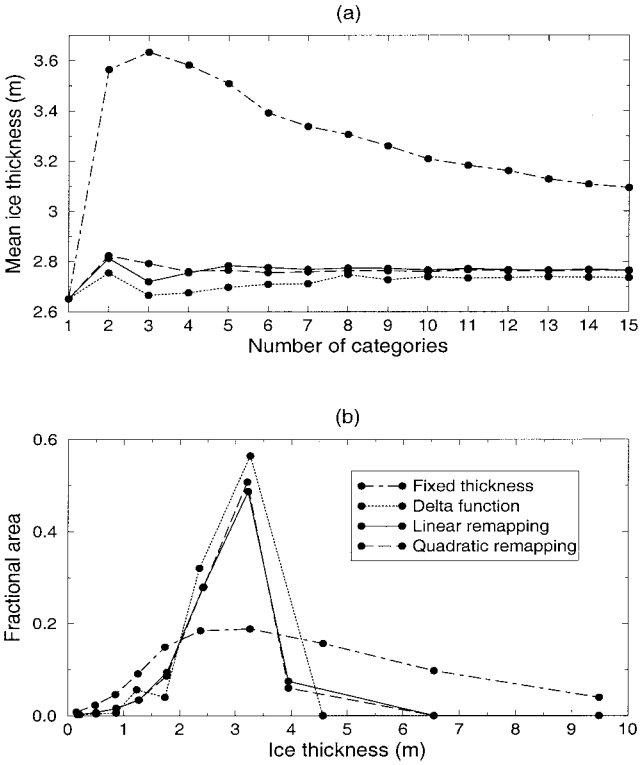

Figure 16. Model results for the four schemes with no ridging, year 100: (a) variation of the annual mean ice thickness with the number of thickness categories and (b) annual mean fractional area in each category with $N = 10$.

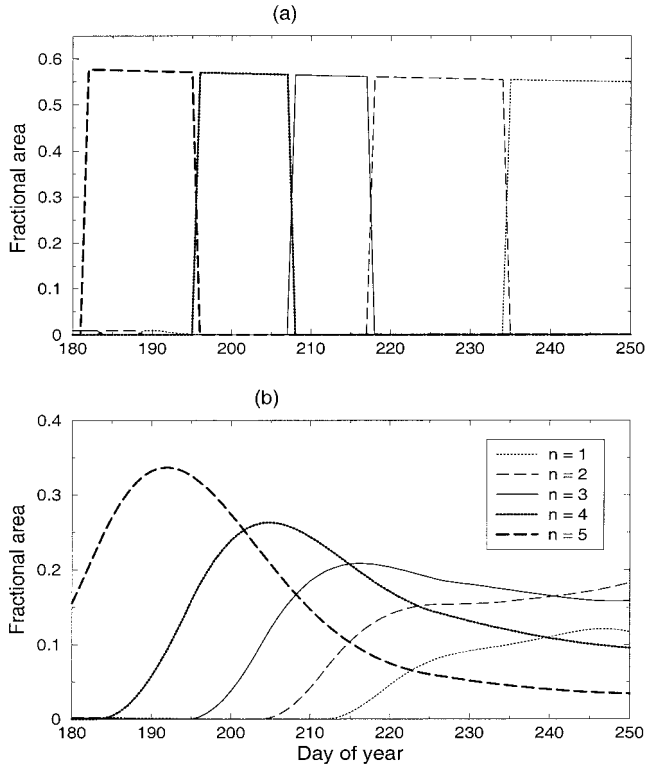

Figure 15. Variation of the fractional area of the thinnest five categories during the summer of year 100 with $N = 12$ and shortwave radiation 5% higher than standard value: (a) delta function scheme and (b) linear remapping.

model simulations with five categories, remapping gives a mean ice thickness within about 10 cm of the asymptotic value. The errors in the mean surface fluxes are <0.1 W m^{-2}, and the ice strength is accurate to within 10%. Increasing N from 5 to 7 can reduce these errors by a factor of 2, but further increases in N make little difference.

These errors are small compared to other model uncertainties. For example, lowering the maximum ice albedo from 0.60 to 0.57 with $N = 15$ and standard forcing reduces the mean ice thickness by 50 cm and raises the shortwave absorption by 1 W m^{-2}. Changing the ridging parameter H^* from 25 to 50 m increases the mean ice strength by more than 50%. Both these modified parameter values are within the range used by current ice models.

Bitz et al. [2001], who used the delta function method, also argued that about five thickness categories are sufficient for climate modeling. With five categories and standard forcing the delta function scheme underestimates the mean ice thickness by about 30 cm and introduces multiyear thickness oscillations of about 15 cm. Although these errors may be tolerable given other model uncertainties, remapping clearly is more accurate.

More categories would be needed in a model that distinguishes among ice types: for example, first-year versus multiyear ice or level versus ridged ice. Then each ice type would have its own thickness distribution, and each distribution would be remapped independently. Since differences between ice types can usually be parameterized in terms of ice thickness, additional thickness distributions would not necessarily improve the results.

Acknowledgments. I thank John Dukowicz for suggesting the application of remapping to the ice thickness distribution and providing extensive guidance. I also thank Cecilia Bitz, Rainer Bleck, Hajo Eicken, Greg Flato, Elizabeth Hunke, Bob Malone, Alan Thorndike, Norbert Untersteiner, and one anonymous referee for helpful reviews. This work was made possible by the support of the DOE Climate Change Prediction Program, a National Science Foundation Graduate Fellowship, and a NASA Global Change Fellowship.

References

Bitz, C. M., and W. H. Lipscomb, An energy-conserving thermodynamic model of sea ice, *J. Geophys. Res*., *104*, 15,669–15,677, 1999.

Bitz, C. M., M. M. Holland, A. J. Weaver, and M. Eby, Simulating the ice-thickness distribution in a coupled climate model, *J. Geophys. Res*., *106*, 2441–2464, 2001.

Bjork, G., On the response of the equilibrium thickness distribution of sea ice to ice export, mechanical deformation, and thermal forcing with application to the Arctic Ocean, *J. Geophys. Res*., *97*, 11,287–11,298, 1992.

Bourke, R. H., and R. P. Garrett, Sea ice thickness distribution in the Arctic Ocean, *Cold Reg. Sci. Technol*., *13*, 259–280, 1987.

Dukowicz, J. K., and J. R. Baumgardner, Incremental remapping as a transport/advection algorithm, *J. Comput. Phys*., *160*, 318–335, 2000.

Flato, G. M., and W. D. Hibler III, Ridging and strength in modeling the thickness distribution of Arctic sea ice, *J. Geophys. Res*., *100*, 18,611–18,626, 1995.

Hibler, W. D., III, Modeling a variable thickness sea ice cover, *Mon. Weather Rev*., *108*, 1943–1973, 1980.

Hunke, E. C., and W. H. Lipscomb, CICE: The Los Alamos Sea Ice Model, documentation and software, Version 2.0, *LA-CC-98-16*, Los Alamos Natl. Lab., Los Alamos, N.M., 1999.

Kwok, R., and D. A. Rothrock, Variability of Fram Strait ice flux and North Atlantic Oscillation, *J. Geophys. Res*., *104*, 5177–5189, 1999.

Lindsay, R. W., Temporal variability of the energy balance of thick Arctic pack ice, *J. Clim*., *11*, 313–333, 1998.

Lipscomb, W. H., Modeling the thickness distribution of Arctic sea ice, Ph.D. thesis, 155 pp., Univ. of Wash., Seattle, 1998.

Maykut, G. A., Large-scale heat exchange and ice production in the central Arctic, *J. Geophys. Res*., *87*, 7971–7984, 1982.

Maykut, G. A., and M. G. McPhee, Solar heating of the Arctic mixed layer, *J. Geophys. Res*., *100*, 24,691–24,703, 1995.

Maykut, G. A., and N. Untersteiner, Some results from a time-dependent thermodynamic model of sea ice, *J. Geophys. Res*., *76*, 1550–1575, 1971.

Perovich, D. K., T. C. Grenfell, B. Light, J. A. Richter-Menge, M. Sturm, W. B. Tucker III, H. Eicken, G. A. Maykut, and B. Elder, *SHEBA: Snow and Ice Studies* [CD-ROM], Joint Off. of Sci. Support, Univ. Cent. for Atmos. Res., Boulder, Colo., 1999.

Rothrock, D. A., The energetics of the plastic deformation of pack ice by ridging, *J. Geophys. Res*., *80*, 4514–4519, 1975.

Schramm, J. L., M. M. Holland, J. A. Curry, and E. E. Ebert, Modeling the thermodynamics of a sea ice thickness distribution, 1, Sensitivity to ice thickness resolution, *J. Geophys. Res*., *102*, 23,079–23,091, 1997.

Thorndike, A. S., D. A. Rothrock, G. A. Maykut, and R. Colony, The thickness distribution of sea ice, *J. Geophys. Res*., *80*, 4501–4513, 1975.

Vinje, T., N. Nordlund, and Å. Kvambekk, Monitoring ice thickness in Fram Strait, *J. Geophys. Res*., *103*, 10,437–10,449, 1998.

W. H. Lipscomb, Los Alamos National Laboratory, Group T-3, Los Alamos, NM 87545. (lipscomb@lanl.gov)

(Received June 30, 2000; revised March 12, 2001;
accepted March 15, 2001.)